# ChemComm

Check for updates

# Strain engineering improves the photovoltaic performance of carbon-based hole-transport-material free CsPbIBr$_2$ perovskite solar cells†

Wei He,‡[a] Xingxing Duan,‡[b] Qunwei Tang, [iD][b] Jie Dou [iD]*[b] and Jialong Duan [iD]*[bc]

Alkylamines with different chain lengths including *n*-butylamine, *n*-hexylamine, and *n*-octylamine, are applied to regulate the CsPbIBr$_2$ perovskite film quality by strain engineering. The status of residual strains is controllably modulated, resulting in improved efficiency and stability of carbon-based hole-transport-material free CsPbIBr$_2$ perovskite solar cells.

In recent years, perovskite solar cells (PSCs) have rapidly become a hot research area due to their low cost and simple preparation. The certified power conversion efficiency (PCE) has achieved 26.1%.[1–3] However, the in-service life of the device has been a limiting factor in promoting the commercialization and industrialization of PSCs. Replacing organometallic halide perovskites with all-inorganic ones is an effective way to enhance the long-term stability of the corresponding solar cells. Note that, compared to organic–inorganic hybrid perovskite films, all-inorganic perovskite films exhibit higher thermal expansion coefficients and phase transition temperatures.[4] The residual stress in perovskite films is determined by various factors during the annealing process, including Young's modulus, Poisson's ratio, the thermal expansion coefficient, and the temperature gradient of both substrate and perovskite. When all-inorganic perovskite films cool from the annealing temperature to room temperature, a large temperature gradient ($\Delta T$) occurs, leading to thermal tensile strain. These strains provide the driving force for defect formation, resulting in non-radiative losses in solar cells, leading to decreased efficiency and increased instability.[5,6] To release tensile strain, the regulation of the crystallization process and light treatment has been employed to release residual stress.[7,8] In addition, Huang *et al.* deposited MAPbI$_3$ films on a flexible substrate with a thermal expansion coefficient close to that of the perovskite crystal,[9] which can significantly reduce thermally induced tensile stress. However, the complex annealing process and uncontrollable stress release mechanism have been still regarded as main limiting factors for their clinical application and industrialization. According to related research, the perovskite crystal structure suffers from the phase transformation from the three-dimensional structure to the single- or multi-layer two-dimensional crystal structure, as the volume of cations increases. This structure is easily formed with long-chain alkyl ammonium. Considering the flexible chain, this additive is expected to play an important role in releasing strain. But, to date, there are few reports on the modulation of stress distribution in inorganic CsPbIBr$_2$ perovskite films using alkylamines with different chain lengths.[10–18]

Herein, we explore the distribution of residual strain profiles in the perovskite films and its effect on photovoltaic performance. We demonstrate that alkylamines with different chain lengths, *n*-butylamine (C$_4$H$_{11}$N, BA), *n*-hexylamine (C$_6$H$_{15}$N, HA), and *n*-octylamine (C$_8$H$_{19}$N, OA) can modulate the residual strain in perovskite film. On one hand, the release of stress is beneficial for reducing defect recombination. On the other hand, alkylamines with different chain lengths based on PSCs lead to suitable energy structures, which facilitate charge transport. Ultimately, the efficiency and stability of carbon-based hole-transport-material-free CsPbIBr$_2$ PSCs are improved.

As shown in Fig. 1a, we fabricated all-inorganic CsPbIBr$_2$ PSCs with FTO/c-TiO$_2$/perovskite/carbon structure and employed these long-chain alkylamines as dopants to investigate the stress regulation of perovskite films. The relevant molecular structure and electrostatic potential are depicted in Fig. S1 (ESI†), with HA exhibiting a slightly stronger electronegativity compared to BA/OA. The mechanism is systematically discussed in the next section. To investigate the interaction mechanism between perovskites and alkylamines, X-ray photoelectron spectroscopy (XPS) measurements were performed as shown in Fig. 1b and Fig. S2 (ESI†). Two main Pb

*[a] Institute of New Energy Technology, College of Information Science and Technology, Jinan University, Guangzhou 510632, P. R. China*

*[b] Institute of Carbon Neutrality, College of Chemical and Biological Engineering, Shandong University of Science and Technology, Qingdao 266590, P. R. China. E-mail: doujiefzu@163.com, duanjialong@sdust.edu.cn*

*[c] Wuhan National Laboratory for Optoelectronics and School of Physics, Huazhong University of Science and Technology, Wuhan 430074, China*

† Electronic supplementary information (ESI) available. See DOI: https://doi.org/10.1039/d4cc01012d

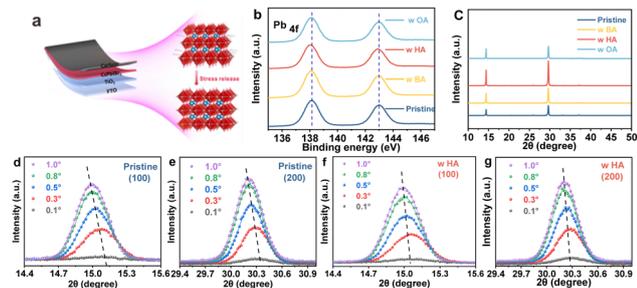‡ These authors contributed equally to this work.

Fig. 1 (a) Schematic diagram of stress control. (b) Pb 4f XPS spectra of perovskite films. (c) XRD and (d)–(g) depth-dependent XRD patterns of perovskite films.

4f peaks of the HA-treated perovskite film are located at 138.00 and 142.89 eV. Compared to the original sample, the peaks from Pb 4f shift to a lower binding energy. It indicates a strong coordination force between the amino group of HA and the $Pb^{2+}$ in the perovskite film. The largest shift for HA-treated perovskite compared to BA and OA cases means the largest interaction. Scanning electron microscopy (SEM) images reveal the surface morphologies of the perovskite films (Fig. S3, ESI†). Doping with different polar molecules has a minimal impact on the crystal size distribution. The effect of alkylamine dopants on the crystal structure and crystallinity of perovskite films was then investigated by X-ray diffraction (XRD) measurement in Fig. 1c. The diffraction peaks at 14.29° and 29.78° correspond to the (100) and (200) facets of $CsPbIBr_2$, respectively. Compared to the pure $CsPbIBr_2$ film, the peak intensity increases after doping treatment, and HA-doped sample exhibits the highest diffraction peak intensity. It means an improved crystallization and reduced defect density. Furthermore, through the grazing incident X-ray diffraction (GIXRD) measurement, we demonstrate the effect of HA modification on the residual stress in the film. As shown in Fig. 1d–g, we explore the stress distribution at different depths within the perovskite films by changing the incident angles ($\omega$) from 0.1° to 0.3°, 0.5°, 0.8° and 1.0°. As $\omega$ increases, the diffraction peaks of the control perovskite film, located at $2\theta$ = 15.05° and $2\theta$ = 30.27°, gradually shift towards the lower angles. This evolution of HA-doped perovskite film is significantly reduced, indicating that the residual stress in the HA-doped perovskite film is released. Therefore, ion migration and phase segregation will be suppressed, and corresponding nonradiative recombination will be inhibited. Thus, the carrier extraction efficiency of the perovskite film is significantly improved.[19–21] To further verify defect reduction, the space charge limiting current (SCLC) measurements were conducted on electron-only devices (FTO/TiO₂/perovskite/PCBM/carbon) in Fig. S4 (ESI†). It displays that the trap-filled limit voltage ($V_{TFL}$) is reduced from 1.558 V in the control one to 1.031 V in the HA-doped device. According to the equation: $N_t = 2\varepsilon_0\varepsilon_r V_{TFL}/qL^2$, where $L$ is the thickness of the perovskite film, $\varepsilon$ is relative dielectric constant, $\varepsilon_0$ is the vacuum permittivity, and $q$ is elementary of electron charge, the defect densities of the control and treated films are calculated to be $1.3 \times 10^{17}$ cm$^{-3}$ and $3.14 \times 10^{16}$ cm$^{-3}$, respectively. HA-treated device exhibits the lowest defect density among all samples.

Steady-state photoluminescence (PL) and time-resolved PL (TRPL) decay curves are presented in Fig. S5 and S6 (ESI†). Compared to the pure $CsPbIBr_2$, the three alkylamine-doped perovskite films exhibit a higher PL emission peak, and the HA-doped perovskite film shows approximately twice the luminescence intensity of the original one. The significant enhancement in PL peak intensity and the prolongation carrier lifetime indicates a reduction in defect density and the suppression of non-radiative recombination in the treated perovskite film. This is beneficial for enhancing carrier transport within the perovskite and at the interfaces over the solar cell.

Bulk composition and stress gradient variation can modulate the energy band structure of perovskite films. To prove the above speculation, we performed ultraviolet photoelectron spectroscopy (UPS) and ultraviolet-visible absorption spectroscopy (UV-vis) measurements to explore the energy levels of perovskite films. Fig. 2a and b exhibit the cut-off edge of the control and doped $CsPbIBr_2$ films. After HA treatment, the cut-off edge value shifts from 17.08 eV to 17.03 eV. The calculations reveal that the Fermi level also rises from −4.12 eV to −4.17 eV. As shown in Fig. 2c and Fig. S7 (ESI†), there is little difference in the light absorption intensity among the various films. The light absorption threshold is basically located at 587 nm, which corresponds to the optical band gap ($E_g$) of about 2.11 eV for $CsPbIBr_2$. Ultimately, these results indicate that the valence band shifts from −6.08 eV to −6.03 eV, and the conduction band from −3.97 eV to −3.92 eV upon the addition of HA. The corresponding energy band structures for the $CsPbIBr_2$ films with and without HA are illustrated in Fig. 2d. After HA treatment, the valence/conduction band positions of $CsPbIBr_2$ shift upward. Compared to the control film, the HA-doped perovskite exhibits better matching with the HOMO energy level of the carbon electron. It improves interfacial charge extraction and inhibits interfacial non-radiative charge recombination.[22,23]
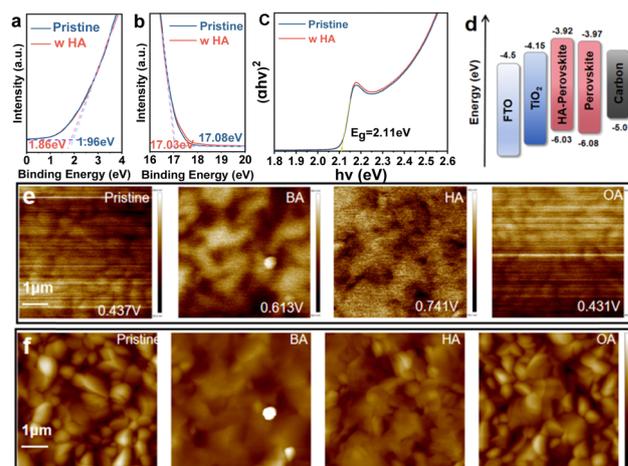


Fig. 2 (a) and (b) UPS spectra of the secondary electron cut-off region and valence band region of the perovskite films. (c) Tauc slope plot calculated from absorption spectra. (d) The energy level obtained from the UPS spectrum. (e) KPFM and (f) AFM images of perovskite films.

For hole-transport-material free devices, the effect of hole transport behavior on the efficiency is greater than that of electron transport behavior. The upward bending of the valence band has a stronger charge carrier transport behavior compared to the conduction band. It could further be verified by the Kelvin probe force microscopy (KPFM) measurements in Fig. 2e, with the potential distribution shown in Fig. S8 (ESI†). The surface potential value of the perovskite film with HA treatment increases compared to the original one. It indicates a decrease in work function, which is consistent with the UPS results. Atomic force microscopy (AFM) was used to assess the morphology and average surface roughness of the perovskite films, as shown in Fig. 2f. The decrease in roughness of the perovskite layer suggests a higher film quality, which attributes to the uniform nucleation and crystallization of the perovskite layer.

To investigate the influence of those alkylamines with different chain lengths on the photovoltaic performance, we fabricated devices with the $FTO/TiO_2/CsPbIBr_2/carbon$ structure. The concentration optimization of the photocurrent density–voltage ($J–V$) curves of PSCs with different alkylamines is shown in Fig. S9 and Table S1 (ESI†). Fig. 3a and Tables S2, S3 (ESI†) present the $J–V$ curves and photovoltaic parameters of the control and alkylamine doped $CsPbIBr_2$ PSCs. Compared to the PCE of 8.33% in the original one, the maximum PCE of PSC with HA treatment is increased to 10.67%. Notably, the photovoltaic performance of the HA-doped device is uniformly and significantly improved in contrast to BA and OA-based devices. The statistical distribution of the measured PCEs for the original and various alkylamine-doped PSCs is also consistent with the above conclusion (Fig. S10, ESI†). We performed external quantum efficiency (EQE) measurement (Fig. 3b) to validate the measured $J_{SC}$. The EQE spectrum of HA-doped PSC is much higher than that of the original one in all absorption regions, especially in the wavelength range from 350 nm to 575 nm. It also is consistent with the result of the $J–V$ measurement. The improved $J_{SC}$ performance might be attributed to a high-quality perovskite with released stress and a suitable energy band structure. The stable power output of the device is obtained, as shown in Fig. 3c. Under external bias near the maximum power output point (1.007 V), the HA-treated PSC exhibits a stable photo-current of 10.20 mA cm$^{-2}$ and an efficiency of 10.67%. Meanwhile, the control $CsPbIBr_2$ device shows relatively poor and unstable photocurrent with an efficiency of 8.33% (the maximum power output point at 0.971 V). To investigate the cause of the increase in open-circuit voltage ($V_{OC}$), we measured the Mott–Schottky curves in Fig. 3d. The HA-doped PSCs exhibit a higher built-in voltage ($V_{bi}$) of 1.64 V compared to the original one (1.51 V). The trend of $V_{OC}$ values is similar to the result obtained from the $J–V$ curve. The plots of $V_{OC}$ as a function of light intensity provide clear insights into the charge recombination mechanisms caused by defects. According to the related literature, the value of the ideal factor ($n$) is closer to 2, and the Shockley-Hall (SRH) recombination is more serious. From the slope of the curve in Fig. 3e, the $n$ of the HA-treated PSC decreases from 1.957 to 1.270. The result shows that the HA-doped PSC significantly reduces trap-assisted recombination, resulting in a more stable $V_{OC}$ under operating condition. Meanwhile, the change in current as a function of light intensity is shown in Fig. S11 (ESI†). In HA-doped device, the value of the ideal factor is close to 1, indicating that the minimal radiative recombination in the cell.[24,25] In addition, Fig. S12 (ESI†) shows the dark $J–V$ curves of original and HA-doped PSCs, proving that the HA-doped PSC exhibits a very small leakage current, as a result, reducing charge recombination loss and ensuring high $V_{OC}$ and fill factor (FF) of the device, and improving the efficiency of the device.[26–28] To better understand the charge transport and recombination in the PSCs, we also obtained the open-circuit photovoltage attenuation curves and derived the carrier lifetime plots in Fig. S13 (ESI†). Among the PSCs with different alkylamines, the HA-doped device shows the largest $V_{OC}$ and smallest decay trend. Compared to the device with other treatments, the charge recombination of HA-doped cell is lower and the carrier lifetime is longer, consistent with the increase in $V_{OC}$. In short, the increase in $V_{OC}$ is owing to the reduction of defects. To further elucidate the charge transport and recombination mechanism of $CsPbIBr_2$ PSCs, electrochemical impedance spectroscopy (EIS) measurements were employed. The related plots of the $CsPbIBr_2$ PSCs doped with different alkylamines are displayed in Fig. 3f. Compared to the original device, the recombination resistance ($R_{rec}$) value of the HA-doped device is significantly reduced. It indicates that the charge transport is promoted and the charge recombination is inhibited. A better interface leads to a higher fill factor (FF). Last but not least, Fig. S14 (ESI†) shows the forward and reverse scans of $J–V$ curves of the original device and HA-doped PSC. The hysteresis factor (HI) of the original PSC is calculated to be 29.9%, while that of the HA-doped one is 18.8%. The reduction in hysteresis is attributed to the decreased defect density of the perovskite and the improved carrier extraction.

Due to the criticality of stability, we investigated the influence of alkyl amines on the stability of the device. The storage
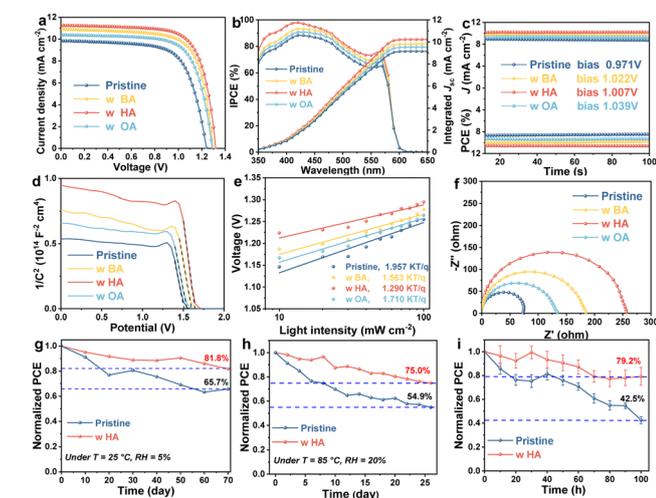


Fig. 3 (a) $J–V$ curves, (b) EQE spectra, (c) steady power output curves, (d) Mott–Schottky plots, (e) $V_{OC}$ upon light intensity curves and (f) Nyquist plots of control and modified group PSCs. Stability performance as a function of the storage time under (g) atmospheric air ($T = 25\ °C$, RH = 5%), (h) high temperature ($T = 85\ °C$, RH = 20%) and (i) 1 sun illumination.

stability of the unpackaged original and doped devices under room temperature and 5% humidity is shown in Fig. 3g and Fig. S15a (ESI†). After aging in the storage environment for 70 days, the PCE of the control device is kept at 65.7% of its original efficiency. Meanwhile, the HA-doped device retains 81.8% of its efficiency under the same aging time. Fig. 3h and Fig. S13b (ESI†) exhibit the thermal stability of PSCs at 85 °C and 20% humidity. After 25 days of aging treatment, the HA-doped PSC still maintains 75% of its original efficiency, while the control device only displays about 54.9% efficiency. Photostability is also shown in Fig. 3i. After aging for 100 h, the original device obtains 42.5% of its original efficiency, while the HA-doped PSC exhibits 79.2% of its original efficiency. We speculate that strain engineering might reduce the defects and inhibit the ion migration of the perovskite film, which significantly improves the stability of the device.

In this paper, three alkylamines with different chain lengths, BA, HA, and OA, were selected to release the internal stress within the perovskite film, adjust the energy level of the device more adaptively, and improve the quality of the perovskite film. After HA-doped treatment, the efficiency of the optimal device was increased from 8.33% to 10.67%, and the long-term stability of the device was also improved. This work shows that stress release and energy band regulation strategies are crucial for achieving long-lasting performance in PSCs, providing a new direction for the commercialization of PSCs in the future.

## Conflicts of interest

There are no conflicts to declare.

## References

1 S. Bai, P. Da, C. Li, Z. Wang, Z. Yuan, F. Fu, M. Kawecki, X. Liu, N. Sakai, J. T.-W. Wang, S. Huettner, S. Buecheler, M. Fahlman, F. Gao and H. J. Snaith, *Nature*, 2019, **571**, 245.
2 Q. Jiang, J. Tong, Y. Xian, R. A. Kerner, S. P. Dunfield, C. Xiao, R. A. Scheidt, D. Kuciauskas, X. Wang, M. P. Hautzinger, R. Tirawat, M. C. Beard, D. P. Fenning, J. J. Berry, B. W. Larson, Y. Yan and K. Zhu, *Nature*, 2022, **611**, 278.
3 Best Research Cell Efficiency Chart, https://www.nrel.gov/pv/cell-efficiency.html.
4 N. Rolston, K. A. Bush, A. D. Printz, A. Gold-Parker, Y. Ding, M. F. Toney, M. D. McGehee and R. H. Dauskardt, *Adv. Energy Mater.*, 2018, **8**, 1802139.
5 C. Ramirez, S. K. Yadavalli, H. F. Garces, Y. Zhou and N. P. Padture, *Scr. Mater.*, 2018, **150**, 36.
6 C. C. Stoumpos, C. D. Malliakas, J. A. Peters, Z. Liu, M. Sebastian, J. Im, T. C. Chasapis, A. C. Wibowo, D. Y. Chung, A. J. Freeman, B. W. Wessels and M. G. Kanatzidis, *Cryst. Growth Des.*, 2013, **13**, 2722.
7 C. Zhu, X. X. Niu, Y. H. Fu, N. X. Li, C. Hu, Y. H. Chen, X. He, G. R. Na, P. F. Liu, H. C. Zai, Y. Ge, Y. Lu, X. X. Ke, Y. Bai, S. H. Yang, P. W. Chen, Y. J. Li, M. L. Sui, L. J. Zhang, H. P. Zhou and Q. Chen, *Nat. Commun.*, 2019, **10**, 815.
8 H. Tsai, R. Asadpour, J. C. Blancon, C. C. Stoumpos, O. Durand, J. W. Strzalka, B. Chen, R. Verduzco, P. M. Ajayan, S. Tretiak, J. Even, M. A. Alam, M. G. Kanatzidis, W. Y. Nie and A. D. Mohite, *Science*, 2018, **360**, 6384.
9 J. J. Zhao, Y. H. Deng, H. T. Wei, X. P. Zheng, Z. H. Yu, Y. C. Shao, J. E. Shield and J. S. Huang, *Sci. Adv.*, 2017, **3**, 5616.
10 Y. Fu, X. Jiang, X. Li, B. Traoré, I. Spanopoulos, C. Katan, J. Even, M. G. Kanatzidis and E. Harel, *J. Am. Chem. Soc.*, 2020, **142**, 4008.
11 M. P. Hautzinger, D. Pan, A. K. Pigg, Y. Fu, D. J. Morrow, M. Leng, M. Y. Kuo, N. Spitha, D. P. Lafayette and D. D. Kohler, *ACS Energy Lett.*, 2020, **5**, 1430.
12 S. Ramos-Terrón, C. Verdugo-Escamilla, L. Camacho and G. de Miguel, *Adv. Opt. Mater.*, 2021, **9**, 2100114.
13 Y. Zhang and N. G. Park, *ACS Energy Lett.*, 2022, 7, 757.
14 X. Zhang, X. Ren, B. Liu, R. Munir, X. Zhu, D. Yang, J. Li, Y. Liu, D. M. Smilgies and R. Li, *Energy Environ. Sci.*, 2017, **10**, 2095.
15 W. Fu, H. Liu, X. Shi, L. Zuo, X. Li and A. K. Y. Jen, *Adv. Funct. Mater.*, 2019, **29**, 1900221.
16 X. Chang, J.-X. Zhong, S. Li, Q. Yao, Y. Fang, G. Yang, Y. Tan, Q. Xue, L. Qiu, Q. Wang, Y. Peng and W.-Q. Wu, *Angew. Chem., Int. Ed.*, 2023, **62**, e202309292.
17 G. Liu, X. Jiang, W. Feng, G. Yang, X. Chen, Z. Ning and W.-Q. Wu, *Angew. Chem., Int. Ed.*, 2023, **62**, e202305551.
18 M. Yang, T. Tian, Y. Fang, W.-G. Li, G. Liu, W. Feng, M. Xu and W.-Q. Wu, *Nat. Sustainability*, 2023, **6**, 1455–1464.
19 H. Bi, B. Liu, D. He, L. Bai, W. Wang, Z. Zang and J. Chen, *Chem. Eng. J.*, 2021, **418**, 129375.
20 H. Wang, C. Zhu, L. Liu, S. Ma, P. Liu, J. Wu, C. Shi, Q. Du, Y. Hao, S. Xiang, H. Chen, P. Chen, Y. Bai, H. Zhou, Y. Li and Q. Chen, *Adv. Mater.*, 2019, **31**, 1904408.
21 H. Bi, Y. Guo, M. Guo, C. Ding, S. Hayase, T. Mou, Q. Shen, G. Han and W. Hou, *Chem. Eng. J.*, 2022, **439**, 135671.
22 D. Luo, W. Yang, Z. Wang, A. Sadhanala, Q. Hu, R. Su, R. Shivanna, G. F. Trindade, J. F. Watts, Z. Xu, T. Liu, K. Chen, F. Ye, P. Wu, L. Zhao, J. Wu, Y. Tu, Y. Zhang, X. Yang, W. Zhang, R. H. Friend, Q. Gong, H. J. Snaith and R. Zhu, *Science*, 2018, **360**, 1442.
23 X. Zheng, Y. Hou, C. Bao, J. Yin, F. Yuan, Z. Huang, K. Song, J. Liu, J. Troughton, N. Gasparini, C. Zhou, Y. Lin, D.-J. Xu, B. Chen, A. K. Johnston, N. Wei, M. N. Hedhili, M. Wei, A. Y. Alsalloum, P. Maity, B. Turedi, C. Yang, D. Baran, T. D. Anthopoulos, Y. Han, Z.-H. Lu, O. F. Mohammed, F. Gao, E. H. Sargent and O. M. Bakr, *Nat. Energy*, 2020, **5**, 131.
24 J. Wang, J. Zhang, Y. Zhou, H. Liu, Q. Xue, X. Li, C. Chueh, H.-L. Yip, Z. Zhu and A. K. Y. Jen, *Nat. Commun.*, 2020, **11**, 177.
25 Y. Zhang, X. Liu, P. Li, Y. Duan, X. Hu, F. Li and Y. Song, *Nano Energy*, 2019, **56**, 733.
26 C. Luo, G. Zheng, F. Gao, X. Wang, Y. Zhao, X. Gao and Q. Zhao, *Joule*, 2022, **6**, 240.
27 Y. Xu, X. Guo, Z. Lin, Q. Wang, J. Su, J. Zhang, Y. Hao, K. Yang and J. Chang, *Angew. Chem., Int. Ed.*, 2023, **62**, 202306229.
28 X. Guo, Z. Lin, W. Cao, Y. Xu, Q. Wang, B. Zhang, Y. Hao and J. Chang, *J. Mater. Chem. C*, 2023, **11**, 9144.